analytica

MDPI

Article

Quantification of PD-1/PD-L1 Interaction between Membranes from PBMCs and Melanoma Samples Using Cell Membrane Microarray and Time-Resolved Förster Resonance Energy Transfer

Lissete Sánchez-Magraner [1], Miguel de la Fuente [2,3], Charles Evans [1], James Miles [1], Ane Elexpe [2,3], Maddalen Rodriguez-Astigarraga [2,3], Egoitz Astigarraga [2] and Gabriel Barreda-Gómez [2,*]

1 Research and Development Division, FASTBASE Solutions, 48160 Derio, Spain; lissete@fastbasesolutions.com (L.S.-M.); chazlink@hotmail.co.uk (C.E.); james.miles@fastbasesolutions.com (J.M.)
2 Research and Development Division, IMG Pharma Biotech, 48160 Derio, Spain; miguel@imgpharma.com (M.d.l.F.); ane@imgpharma.com (A.E.); maddalen@imgpharma.com (M.R.-A.); egoitz.astigarraga@imgpharma.com (E.A.)
3 School of Medicine and Nursing, University of the Basque Country UPV/EHU, 48940 Leioa, Spain
* Correspondence: gabriel.barreda@imgpharma.com; Tel.: +34-94-4316577; Fax: +34-94-6013455

Citation: Sánchez-Magraner, L.; de la Fuente, M.; Evans, C.; Miles, J.; Elexpe, A.; Rodriguez-Astigarraga, M.; Astigarraga, E.; Barreda-Gómez, G. Quantification of PD-1/PD-L1 Interaction between Membranes from PBMCs and Melanoma Samples Using Cell Membrane Microarray and Time-Resolved Förster Resonance Energy Transfer. *Analytica* **2021**, *2*, 156–170. https://doi.org/10.3390/analytica2040015

Academic Editors: Marcello Locatelli, Victoria Samanidou, Roberto Mandrioli and Thomas W. Bocklitz

Received: 30 July 2021
Accepted: 7 October 2021
Published: 13 October 2021

Abstract: Melanoma is a carcinoma known to evade the host immune defenses via the downregulation of the immune response. One of the molecules involved in this mechanism is programmed cell death ligand 1 (PD-L1), which interacts with its receptor, programmed cell death protein 1 (PD-1), expressed on T cells, leading to a reduction in cytokine release and cytotoxic activity, as well as a halt in T-cell proliferation. The approved therapeutic monoclonal antibodies, such as pembrolizumab, target the PD-1/PD-L1 interaction and are revolutionizing cancer treatments. We developed an assay that provides a quantitative readout of PD-1/PD-L1 interactive states between cell membranes of human immune cells (peripheral blood mononuclear cells, PBMCs) and PD-L1-expressing samples. For this purpose, cell membrane microarrays (CMMAs) were developed from membranes isolated from a HT144 cell line and melanoma samples, and PD-L1 expression was quantified using immunofluorescence (IF). CMMAs were incubated with cell membranes of PBMCs expressing PD-1, and the interaction with PD-L1 was quantified by time-resolved Förster resonance energy transfer, in the presence and absence of pembrolizumab as a blocking drug. The developed assay was able to quantify the PD-1/PD-L1 interaction, and this engagement was disrupted in the presence of the blocking antibody. This demonstrates the potential of the method to analyze monoclonal antibody drugs, as well as the functional states of immune checkpoint regulators. Furthermore, our findings provide evidence to support the future implementation of this methodology for both drug discovery and immune system monitoring in cancer, transplantation, and inflammatory and autoimmune diseases.

Keywords: immunotherapy; protein–protein interaction; melanoma; microarray; amplified FRET; PD-L1/PD-1; immune checkpoint inhibitors

1. Introduction

Protein–protein interactions are important signaling events in pathologies such as autoimmune disease, inflammation, transplant rejection, and cancer. Melanoma, non-small-cell lung carcinoma (NSCLC), and clear-cell renal cell carcinoma (ccRCC) are amongst a subset of carcinomas known to evade the host immune defenses via the manipulation of the immune system, leading to the downregulation of the immune response against the tumor. Key players in developing this adaptive immune resistance are programmed death receptor 1 (PD-1) and its complementary ligand, programmed death ligand 1 (PD-L1). PD-1 is a single-pass type I membrane protein with 288 residues, which is expressed on

T cells, B cells, and NK cells, among others; its expression is upregulated on exhausted T cells. PD-L1 is also a single-pass type I membrane protein with 290 residues, which is overexpressed in different types of cancer, including melanoma, lung, and kidney, in an inflammation-dependent manner. The interaction of PD-1 with its ligand results in reduced cytokine release and cytotoxic activity and halted T-cell proliferation [1–5].

Immunotherapy targeted against PD-1/PD-L1 has revolutionized cancer treatments, and anti-PD-1 therapies (nivolumab/pembrolizumab) have improved clinical outcomes in many cancers, such as advanced melanoma. However, approximately 60–70% of patients do not respond, possibly due to intrinsic resistance or the absence of T cells in the tumor; these patients would not experience benefit from anti-PD-1 blockade [6]. Response rates to immune checkpoint inhibitor (ICI) treatment for many tumors fall within 20% to 40%. Thus, the primary resistance or nonresponse to ICIs clearly remains a critical issue [5].

Tumor cell PD-L1 expression levels are currently the most commonly used biomarker in cancer. A high expression of PD-L1 in tumor cells is usually associated with a more aggressive tumor phenotype and supports its role in immune escape; however, in some cancers, such as malignant melanoma and ccRCC, this paradigm has not proven to be as relevant as in other neoplasia, such as lung cancer. Indeed, tumor PD-L1 expression alone is considered to be a poor predictive marker of efficacy outcomes in this population and, alone, cannot be used for patient selection [7–9]. This could be due to intrinsic resistance or the absence of T cells in the tumor [6,10].

The ability to investigate proteins and their interactions in cells and tissues can offer profound insights into the function of cellular processes and the alterations of normal processes in disease. A novel antibody-based assay to quantify the PD-1/PD-L1 interaction in cell cultures and malignant tissue samples was developed and tested. It is an imaging assay that provides a quantitative readout of protein–protein interaction between cells at a 10 nm distance. iFRET (immune-FRET) employs a two-site, cell–cell amplified Förster resonance energy transfer (FRET) method, detected by fluorescence lifetime imaging microscopy (FRET/FLIM), enabling stringent patient stratification to immunotherapy [11].

CMMA can be used to support membrane protein studies [12], since the integrity of the cell membrane and the conservation of the lipid environment remain stable, allowing a physiological analysis of receptor functional states [13]. It should be noted that CMMA has already been successfully used in several studies to measure the expression and functional activity of membrane proteins [13–15]. In addition, this miniaturized high-throughput tool allows the use of scarce samples to generate hundreds of microarrays that can be employed to perform consecutive analyses. Thus, this technology enables the simultaneous determination of the expression and interaction of PD-1/PD-L1 in different types of samples, using a single assay and the small amount of sample available. The PD-1/PD-L1 interaction was quantified using CMMA derived from cell lines and tumor samples were incubated with PBMC membranes in the presence and absence of pembrolizumab as a blocking drug. The different levels of interaction were determined on the basis of FRET efficiency values.

PD-1/PD-L1 interaction was used as a molecular model for protein–protein interaction assessment in CMMA co-incubated with PBMC membranes. Our findings illustrate a novel strategy for quantifying protein–protein interactions in model membranes without the need for living cells. The obtained results revealed that the PD-1/PD-L1 interaction can be detected using the assay developed based on iFRET, PBMC membranes, and CMMA from cell lines and melanoma samples. Thus, the method opens a new approach to quantifying protein–protein interactions, using this model membrane system for monitoring patient immune response. This assay could, a priori, be used to stratify patients in any immune-dysregulated pathology, such as cancer, autoimmune diseases, inflammation, and transplant rejection.

2. Materials and Methods

2.1. Antibodies and Reagents

Monoclonal antibodies, mouse anti-hPD-1 (ab52587), and rabbit anti-hPD-L1 (ab205921) were purchased from Abcam (Cambridge, UK). Pierce endogenous peroxidase suppressor (35,000), an Alexa Fluor Tyramide SuperBoost Kit (B40925), and Prolong Glass antifade mount (P36984) were obtained from Thermo Fisher Scientific (Waltham, MA, USA). AffiniPure F(ab′)2 fragment donkey anti-mouse IgG and peroxidase-conjugated AffiniPure F(ab′)2 fragment donkey anti-rabbit IgG were purchased from Jackson Immuno Research Laboratories (Baltimore, PA, USA). ATTO 488 NHS ester was purchased from Merck and was conjugated to the AffiniPure F(ab′)2 IgG, as described [15].

2.2. Tissue Samples and Reagents

The samples used for CMMA construction were the HT144 cell line, human melanoma samples, and rat brain cortex tissue. The samples were obtained, respectively, from AMS-BIO (Abingdon, UK) and the University of the Basque Country (UPV/EHU, Leioa, Spain); PBMCs used for the study of PD-1/PD-L1 interaction were also acquired from AMS-BIO (Abingdon, UK). When obtained, all samples were treated as described below for membrane extraction.

2.3. Cell Membrane Microarray

The microarrays were composed of a collection of cell membrane homogenates isolated from a biopsy of human melanoma samples, HT144 human cells, and rat cerebral cortex tissue. Membrane homogenates were obtained following established protocols [16,17]. Briefly, samples were homogenized using a Teflon-glass grinder (Heidolph RZR 2020) or a disperser (Ultra-Turrax T10 basic, IKA) in 20 volumes of homogenized buffer (1 mM EGTA, 3 mM $MgCl_2$, and 50 mM Tris-HCl, pH 7.4) supplemented with 250 mM sucrose. The crude homogenate was subjected to a 1500× *g* centrifugation (AllegraTM X 22R centrifuge, Beckman Coulter) for 5 min at 4 °C, and the resultant supernatant was centrifuged at 18,000× *g* (Microfuge 22R centrifuge, Beckman Coulter) for 15 min (4 °C). The pellet was washed in 20 volumes of homogenized buffer and re-centrifuged under the same conditions, once at 1500× *g* and then the supernatant at 18,000× *g*. The tubes were finally decanted, and the pellets containing the membrane homogenates were frozen at −80 °C, except for one aliquot, which was used to determine the protein concentration. The protein concentration was measured using the Bradford method [13,18] and adjusted to 10 mg/mL for microarray printing.

The membrane homogenates of each sample were resuspended in buffer and printed (7 nL/spot) onto glass slides using a noncontact microarrayer (Nanoplotter NP 2.1) with a piezoelectric tip. Before the printing step, the slides were activated with an acid treatment to make the surface hydrophobic, and washed, dried, and stored at 20 °C (EP2048534A4). Three replicates of the three samples (rat cortex, HT144, and melanoma) were printed in each CMMA. Two CMMAs were printed on each slide, in order to adapt the microarray format to the conventional tools used in low density tissue microarray experiments. The printing was carried out under controlled humidity (60%) at 4 °C, and CMMAs were stored at −20 °C until usage. A total of 80 microarrays were printed for the optimization of the PD-1/PD-L1 interaction assay, as well as for the quality control analyses. For this purpose, lipidomic analysis, functional coupling assays of two GPCRs (cannabinoid CB1 and histamine H4 receptors), and immunodetection of histamine H4 receptors were performed using consecutive microarrays for PD-1/PD-L1 interaction (Appendix A).

2.4. Time-Resolved Immune-Amplified Förster Resonance Energy Transfer (iFRET) Detected by Fluorescence Lifetime Imaging Microscopy (FLIM)

iFRET relies on a two-site labeling assay, in which two primary monoclonal antibodies are used to detect the receptor (PD-1) and ligand (PD-L1). These antibodies are then stained with Fab fragments conjugated to the donor chromophore: ATTO488 for PD-1, and

horseradish peroxidase (HRP) for PD-L1. Tyramide signal amplification is then used to label HRP with the acceptor chromophore ALEXA594. The conjugation of the chromophores to Fab fragments, which bind to the two primary antibodies, allows the critical FRET distance of 10 nm or less to be maintained and provides the appropriate tool for measuring protein–protein interactions.

A Nikon Eclipse Ti widefield light microscope with multiple-frequency-domain FLIM (Lambert Instruments) was used to carry out all acquisitions. The excited-state lifetime of the donor fluorophore (ATTO488) was measured in the absence and presence of the acceptor fluorophore, termed the donor only (τD) and donor/acceptor (τDA), respectively. Excitation sources included both a 40 MHz modulated 473 nm diode laser and a mercury (Hg) source with a TRITC filter for ATTO488 and ALX594 fluorophores, respectively. The 473 nm laser provided both donor intensity and lifetime (τ measurements, while Hg readouts simply provide acceptor intensities). The experiments were performed using a 63× Nikon Apo TIRF objective with a numerical aperture (NA) of 1.49. The acquisition parameters were an exposure time of 250 ms and a peak power of 32 mW for the 473 nm laser, while, for the Hg source, the exposure time was 10 ms.

Using a semiautomated, high-throughput mfFLIM platform from FASTBASE Solutions S.L. (Derio, Spain), each region of interest in the CMMA was mapped according to its *XY*-coordinates on the slide, thus generating a mapping file [19,20]. Phase lifetimes, average intensities, and lifetime images were calculated automatically. A decrease in donor lifetime (τ_D) in the presence of the acceptor chromophore (τ_{DA}) is indicative of resonance energy transfer. FRET efficiency (E_f %) values were calculated using the following equation, where τ_D and τ_{DA} are the lifetimes of the donor in the absence and presence of the acceptor, respectively:

$$Ef(\%) = \left[1 - \left(\frac{\tau DA}{\tau D}\right)\right] \times 100. \quad (1)$$

2.5. FRET-FLIM Assay for PD-1/PD-L1 Interaction in Cell Membrane Microarrays

CMMAs with human PD-L1-embedded membranes were performed using cell membranes isolated from a melanoma biopsy, HT144 cell line, and, as a negative control, rat cortex. CMMAs were incubated overnight at 37 °C in a humidified chamber with cell membranes isolated from human PBMCs in the presence and absence of 25 µg/mL of pembrolizumab (anti-PD-1 blocking antibody) to inhibit PD-1/PD-L1 interactions. The membranes of the PBMCs were isolated following the protocol previously detailed in the Cell Membrane Microarray section.

The unbound membranes were removed, and CMMAs were washed twice for 5 min with phosphate-buffered saline (PBS). They were fixed with 4% paraformaldehyde (PFA) for 12 min. The PFA was then removed, and the CMMAs were washed thrice for 5 min with PBS. CMMAs were then incubated with endogenous peroxidase suppressor from Thermo Fischer (35,000, Waltham, MA, USA), for 30 min at room temperature (RT), to quench the endogenous peroxidases. Then, they were washed with PBS and subsequently incubated with 1% (10 mg/mL) bovine serum albumin (BSA) for 1 h at RT. Therefore, slides were washed thrice in PBS. Two consecutive CMMAs were labeled, one with the donor antibodies and the other with both donor and acceptor antibodies.

Primary antibody staining was carried out by adding mouse anti-PD-1 (1:100 in BSA) to the donor only (D) slide. Meanwhile, the donor acceptor (D/A) slide was labeled with both mouse anti-PD-1 (1:100 in BSA) and rabbit anti-PD-L1 (1:500 in BSA). The CMMAs were incubated overnight at 4 °C with the antibodies. Then, they were washed twice with PBS containing 0.02% Tween-20 (PBST). Secondary Fab fragments were added; the D slides were labeled with anti-mouse FabATTO488 (1:20), and the D/A slides were labeled with FabATTO488 (1:20) and anti-rabbit FabHRP (1:200). The CMMAs were incubated for 2 h at RT, and then washed twice with PBST and once with PBS.

Tyramide signal amplification (TSA) was performed on the D/A slides at RT in the dark, via the addition of Alexa594-conjugated tyramide diluted in reaction buffer (1:100) in

the presence of H_2O_2. The reaction was stopped after 20 min using the reaction stop buffer, and the CMMAs were washed thrice with PBS. All CMMAs were then mounted using a Prolong Glass anti-fade mount and allowed to cure overnight at RT, protected from light.

2.6. Data Normalization

The protein content of the membrane homogenates was measured using the Coomassie brilliant blue protein-binding method [17], with bovine serum albumin as a standard. After printing membrane homogenates on the slides, the protein concentration was recalculated using the Bradford method adapted to CMMAs. Briefly, CMMAs were dried for 15 min and incubated in 50 mM Tris-HCl buffer (pH 7.4) for 15 min. CMMAs were subsequently incubated in Coomassie brilliant blue solution for 60 min at RT, washed in 50 mM Tris-HCl buffer for 15 min (2×), and dried at RT. Slides images were acquired using a scanner (Epson Perfection V750 Pro) and quantified using the software ImageScanner (IMG Pharma, Derio, Spain). Data were processed with GraphPad Prism 5.00 (GraphPad Software, San Diego, CA, USA).

2.7. Data Analysis

CMMA fluorescent signals were acquired using a ChemiDoc Imaging System (BioRad, Universal Hood 3) with Green EPI laser illumination and a 610/620 nm filter, followed by quantification using the software ImageScanner (IMG Pharma, Derio, Spain). Data were processed with GraphPad Prism 8.00 (GraphPad Software, San Diego, CA, USA).

Statistical analysis was conducted and box-and-whisker plots were generated using Origin Pro8. Statistical differences were calculated between conditions using a Mann–Whitney U test (values indicated on the box-and-whisker plots). The Mann–Whitney U test is a nonparametric test and, thus, does not assume a normal distribution of results. The box-and-whisker plots present the 25–75% (box) and the 1–99% (whiskers) ranges. Statistical differences are indicated with p-values ≤ 0.05.

3. Results

In order to study the PD-1/PD-L1 interactions between PD-1 expressed in PBMCs and PD-L1 in HT114 cells and melanoma samples, CMMAs were developed, and the PD-L1 expression was quantified by IF. PD-1/PD-L1 interactions were then assessed by incubating CMMAs with PBMC membranes in the absence and presence of a saturating concentration of the blocking antibody, pembrolizumab, using iFRET and the developed protocol (Figure 1).

3.1. PD-L1 Is Expressed in Melanoma and HT144 Cell Membranes

Human PD-L1 expression was assessed in the samples immobilized in the CMMAs, using an anti-hPD-L1 IgG labeled with a fluorescent secondary antibody, and the signal intensity was quantified. A high specific binding for anti-PD-L1 was observed in HT144 cells and melanoma samples, whereas it did not exceed nonspecific binding in rat cerebral cortex tissue (Figure 2).

HT144, melanoma, and rat cortex had mean fluorescence intensities of 39,123 ± 17,541 a.u., 39,020 ± 9513 a.u., and 9398 ± 5052 a.u., respectively. Once the PD-L1 expression was quantified in the target samples (Figure 2), the interaction of this ligand with its receptor, PD-1, in human PBMCs was quantified using iFRET.

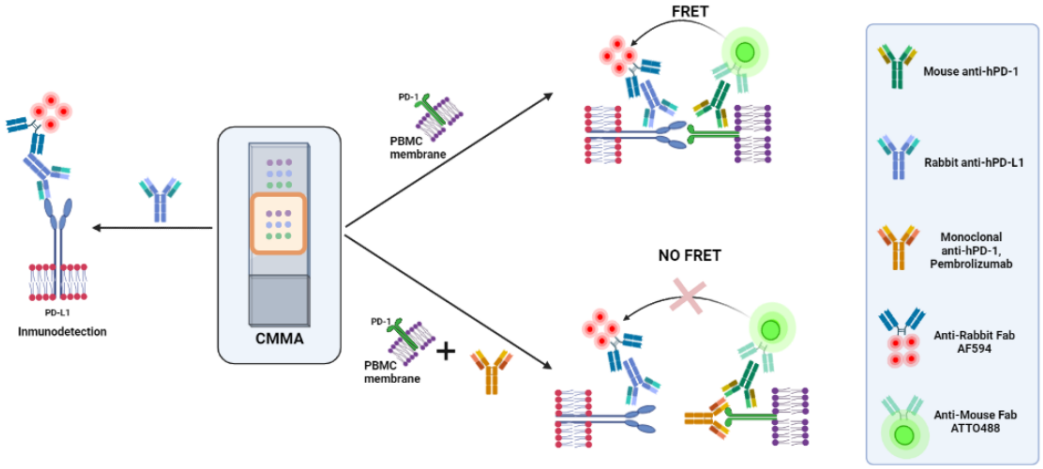

Figure 1. Two types of assays were performed. On the left, quantification of PD-L1 protein expression by IF. On the right, two types of FRET assay were performed for the quantification of PD-1/PD-L1 in the absence (upper) and presence (bottom) of a saturating concentration of the blocking antibody, pembrolizumab. Only one CMMA is represented as an example; each slide had two CMMAs printed. Created with BioRender.com.

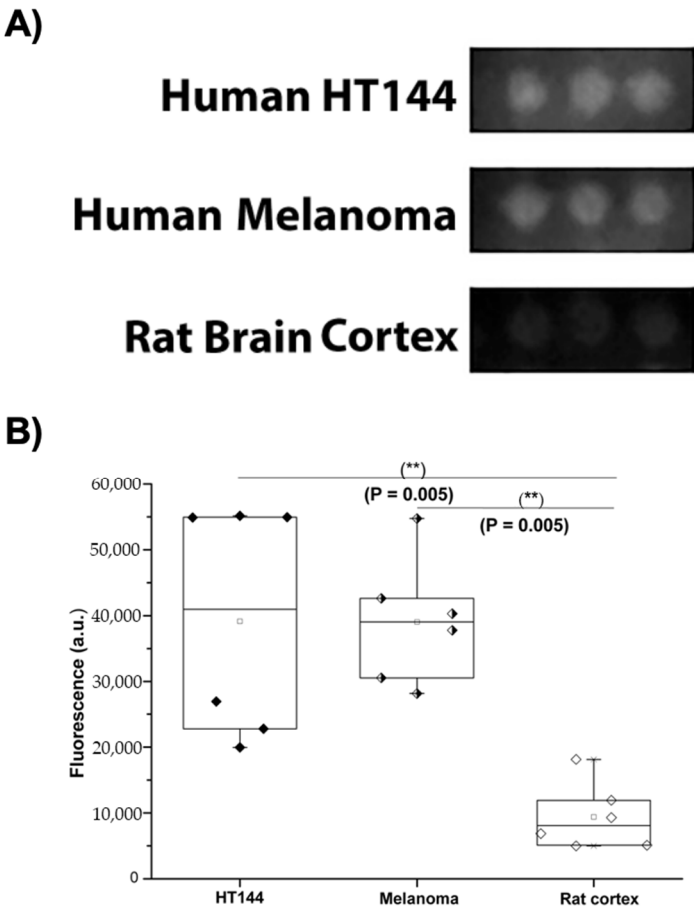

Figure 2. PD-L1 expression in melanoma and HT144 cell membranes. (**A**) Fluorescent signal intensity of Alexa Fluor 594 fluorophore conjugated with anti-PD-L1 antibody detected in melanoma samples and HT144 cells versus rat cerebral cortex tissue. (**B**) Box-and-whisker plot of quantified fluorescent intensity of the three samples: HT144 (black diamonds), human melanoma (black and white diamonds), and rat brain cortex (white diamonds); ** $p < 0.01$.

3.2. PD-1/PD-L1 Specific Interaction Is Quantified in CMMAs Incubated with PBMC Membranes Using iFRET

CMMAs were originally designed for immunolabeling assays without co-incubation with other cell membranes. Thus, CMMA protocols were adapted for the iFRET assay in order to quantify PD-1/PD-L1 interactions in the presence and absence of a saturating concentration of the blocking antibody, pembrolizumab. PD-1/PD-L1 interactions were assessed in HT144 melanoma cells, melanoma patient samples, and rat brain cortex membranes as a negative control, following the incubation of these CMMAs with cell membranes isolated from PBMCs.

Figure 3A shows the PD-1/PD-L1 interaction in CMMAs from the HT144 melanoma cell line incubated with PBMC membranes in the presence and absence of pembrolizumab. The FLIM images consist of pseudo-color lifetime maps, where blue indicates a higher lifetime (3.2 ns) and red indicates a lower lifetime (1.4 ns). The grayscale intensity maps demonstrate the expression of PD-1 (donor) and PD-L1 (acceptor). In the absence of pembrolizumab, the lifetime decreased from 2.34 $\pm$ 0.12 ns to 2.00 $\pm$ 0.13 ns, resulting in a FRET efficiency of 14.53% (Figure 3A, upper panel). However, in the presence of 25 μg/mL pembrolizumab, no reduction in donor lifetime in the presence of the acceptor was observed, yielding a FRET efficiency of 0% (Figure 3A, bottom panel). The same experiment was carried out using melanoma tissue membrane microarrays incubated with PBMC membranes in the presence and absence of pembrolizumab (Figure 3B). Here, in the absence of the blocking drug, donor lifetime decreased from 2.57 $\pm$ 0.08 ns to 2.30 $\pm$ 0.16 ns, resulting in a FRET efficiency of 10.51% (Figure 3B, upper panel). Contrastingly, in CMMAs treated with pembrolizumab, no change in the donor lifetime in the presence of the acceptor occurred, resulting in a FRET efficiency of 0% (Figure 3B, bottom panel). No interactions occurred when CMMAs were not incubated with PBMCs; therefore, FRET signals in all the conditions tested were 0%. These results indicate that the decreases in donor lifetimes, reflected by the high FRET efficiency values, were due to the specific interactions of PD-1 expressed in PBMCs and PD-L1 present in CMMAs. In both cases (Figure 3A,B), intensity maps confirmed the presence of the donor, PD-1, and acceptor, PD-L1. These findings suggest that PD-1/PD-L1 interactions can be quantified by the assay developed using iFRET. Notably, when the blocking drug, pembrolizumab, is present, this receptor/ligand interaction is disrupted, and FRET does not occur.

Three replicates per sample type were analyzed in the presence and absence of pembrolizumab, and the mean FRET efficiency for each sample type was calculated. Box-and-whisker plots were created for all CMMA cores assessed, and the FRET efficiencies obtained were significantly higher in the absence of pembrolizumab with mean values of 10.05% $\pm$ 1.19% and 3.74% $\pm$ 1.33% for HT144 and melanoma samples, respectively (Figure 4A,B). In the presence of pembrolizumab, PD-1/PD-L1 interactions were abolished, and, therefore, all FRET efficiencies were 0% in both sample types. Mann–Whitney U analysis was performed to determine statistical differences between pembrolizumab-treated and untreated CMMAs (statistical differences are indicated with p-values ≤ 0.05). FRET efficiency values were significantly higher in the absence of blocking antibody for HT144 (*** $p = 1.03 \times 10^{-5}$) and melanoma (** $p = 0.007$) compared to CMMAs treated with 25 μg/mL of the blocking drug. The rat cerebral cortex CMMA was used as a negative control; therefore, no significant differences were detected between the treated and untreated samples, with mean FRET efficiencies of 0.60% $\pm$ 0.42% and 0.92% $\pm$ 0.28% in the absence and presence of pembrolizumab, respectively (Figure 4C). These results demonstrate that the iFRET assay, using a CMMA model system incubated with PBMCs, is able to quantify the PD-1/PD-L1 interactions at distances of 1–10 nm. The ranges of FRET efficiency values obtained here are similar to previous results using cell cultures and melanoma patient samples [11].

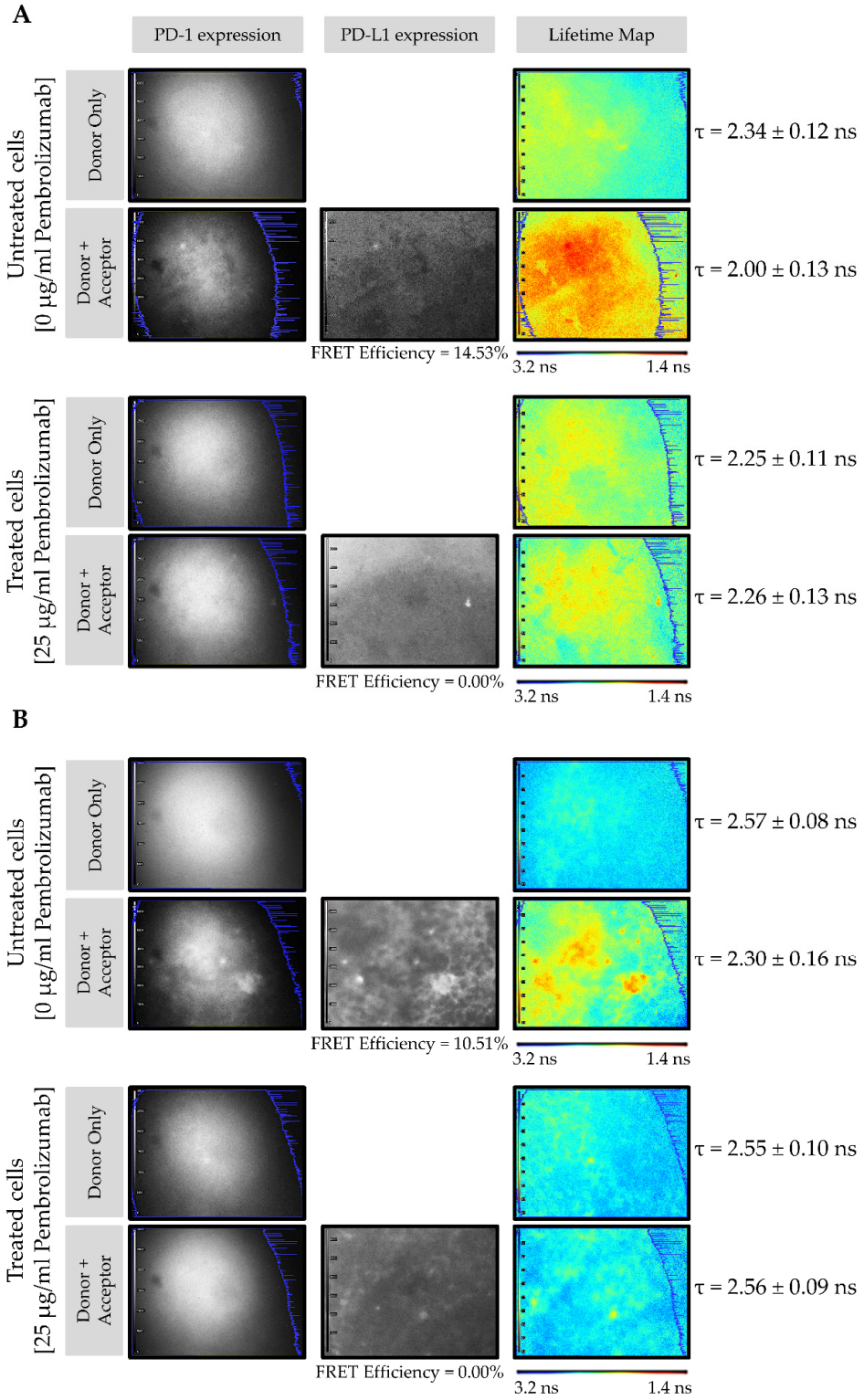

Figure 3. iFRET detects and quantifies the PD-1/PD-L1 interaction in CMMAs incubated with human PBMC membranes in the presence and absence of pembrolizumab. FLIM images of the CMMAs from HT144 cells (**A**) and melanoma samples (**B**) incubated with PBMC membranes in the presence (bottom) and absence (upper) of pembrolizumab. The grayscale intensity maps indicate the expression of PD-1 (donor, ATTO488) and PD-L1 (acceptor, ALEXA594). The pseudo-color lifetime maps indicate the lifetime of the donor (τ), in the presence and absence of the acceptor, wherein blue indicates a higher lifetime and red indicates a lower lifetime.

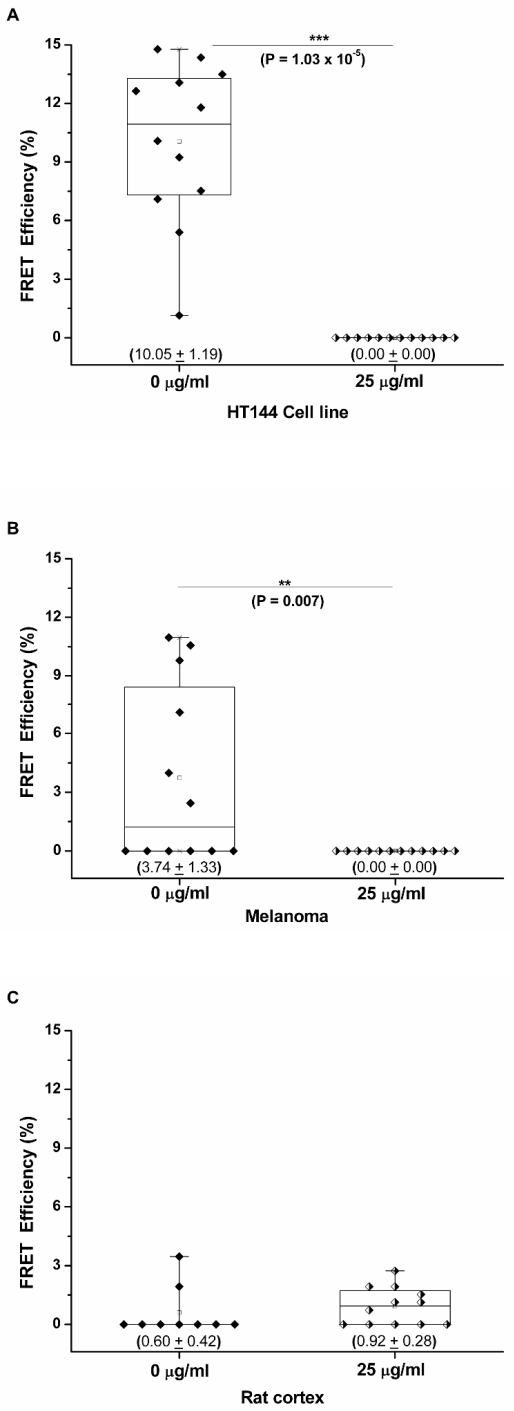

Figure 4. Pembrolizumab inhibits the PD-1/PD-L1 interaction in melanoma and HT144 cell membranes incubated with human PBMCs. Box-and-whisker plot showing the distribution of FRET efficiencies in three types of membrane samples: HT144 cells (**A**), melanoma samples (**B**), and rat cerebral cortex tissue as a negative control (**C**), in the presence and absence of the anti-PD-1 blocking antibody, pembrolizumab. These plots show all FRET efficiencies (interaction states) observed in each sample type with mean FRET efficiencies ± SEM indicated in parentheses. Mann–Whitney U analysis was performed to determine statistical differences between pembrolizumab-treated and untreated CMMAs (statistical differences are indicated with p-values ≤ 0.05). FRET efficiency values were significantly higher in the absence of blocking antibody for HT144 (*** $p = 1.03 \times 10^{-5}$) and melanoma (** $p = 0.007$) compared to CMMAs treated with 25 μg/mL of the blocking drug.

4. Discussion

We developed CMMAs using membranes isolated from the human melanoma cell line, HT144, as well as from a human biopsy of primary melanoma, together with membrane preparations from rat cerebral cortex tissue. This microarray technology maintains the function of receptors, enzymes, and other proteins, providing a powerful tool for the screening of drugs and antibodies. To this end, several assays, including radioligand binding studies, enzymatic analyses, and immunoassays, have been performed using CMMAs [13–15] (Appendix A); however, to date, none have been used to study membrane–membrane interactions using proteins expressed in membranes in close proximity.

HT144 is a malignant human melanoma cell line that displays an aneuploid fibroblastic morphology and grows in adherent tissue culture [20]. These cells present an elevated expression of PD-L1 [21] (Figure 2), due to their cancerous origin [22]. Furthermore, the human melanoma samples presented high levels of PD-L1 (Figure 2). This is a well-known characteristic of this subset of skin cancer [23], which is associated with worsened tumor prognosis, reduced immune response, and neoplastic progression [24]. As a non-expressing non-human PD-L1 sample, rat brain cortex was used. These negative control samples did not present a significant fluorescent signal (Figure 2), in line with the specificity of the anti PD-L1 mAb for the human PD-L1 protein.

The results obtained suggest that the PD-1/PD-L1 interactions can be detected by iFRET using model membrane systems such as CMMAs, and that these interactions are abolished in the presence of the anti-PD-1 blocking drug, pembrolizumab (Figures 3 and 4). These findings highlight the specificity and sensitivity of the developed assay using iFRET and agree with previous reports using the iFRET methodology [12]. These findings assessed PD-1/PD-L1 interaction states in single-cell assays using ccRCC, primary malignant melanoma, and metastatic NSCLC biopsies, wherein PD-1/PD-L1 interaction levels have predictive power with respect to patient response to anti-PD-1 blocking drugs [11]. Another antibody-based fluorescent technique used to determine protein–protein interaction is the duolink proximity ligation assay (PLA) from Merck, based on the method developed by Soderberg et al. [25]. PLA, as opposed to iFRET ($d < 10$ nm), detects distances of tens of nm [26]; however, a previous study comparing PLA with iFRET for assessing PD-1/PD-L1 interaction provided evidence that PLA did not perform as well as iFRET in identifying the PD-1/PD-L1 interaction [11].

Furthermore, the binding assays between the receptor, PD-1, and the ligand, PD-L1, expressed in PBMCs and melanoma cells, respectively, demonstrated for the first time that CMMAs can be used to evaluate immune recognition pathways. These membranes thaw and acclimatize faster than conventional techniques with living cells, with a consequent reduction in time and labor. Microarray technology allows the production of homogeneous CMMAs with a reduced amount of sample, providing a stable measure of adaptive immune resistance that can be monitored through time.

CMMAs present some advantages when compared to other methods of detecting PD-1/PD-L1 interactions, due to their characteristics as a high-throughput, miniaturized, and parallelizable analysis tool. First of all, the amount of sample used is minimal, allowing the user to spare valuable tissue biopsies. Thus, the CMMA provides a precision tool for the production of large batches of microarrays from smaller sample quantities than required by a conventional assay. This technology allows optimizing the study of scarce samples, such as the human melanoma used in this work. Furthermore, different types of assays can be conducted, in order to assess the CMMA functionality as a quality guarantee (Appendix A). Mass spectrometric analysis of the lipid profile of each sample printed on the microarray can be acquired to study the lipid environment (Appendix A, Figure A1). The G-protein-coupled receptor functionality can be assayed using [^{35}S]GTPγS, in addition to its expression using immunochemistry techniques (Appendix A, Figure A3). The potential of developing different studies with CMMAs makes them a powerful tool for drug mechanism studies, drug and biomarker discovery [27], toxicity studies [28], and different high-throughput omics analyses [29], among others. Methods such as coimmunoprecip-

itation can be used to determine protein–protein interactions, and the abovementioned analysis can be developed using classic biomolecular techniques, such as high-performance liquid chromatography to study lipidic profiles, or Western blot for biomarker discovery. Multi-well plate assays or dot-blot analysis also represent alternative methods; however, as with the other techniques listed, a higher amount of sample is required and no miniaturization of the process is possible, while additional membrane analysis cannot be carried out (Appendix A).

This is the first assay developed to quantify membrane–membrane interactions using proteins expressed in membranes that are immobilized in a microarray format. Moreover, the study of other protein–protein interactions can be of great interest for immune monitoring, such as cytotoxic T-lymphocyte antigen-4 (CTLA-4) and CD80/86 for immune suppression, or HLA Class I/$CD8^+$ T cells and HLA Class II/$CD4^+$ T cells for immune activation. Thus, this technology opens a new field for monitoring the immune system in transplant rejection, as well as inflammatory, or autoimmune diseases.

5. Conclusions

The results, using PD-1/PD-L1 as an example of ligand–receptor binding, demonstrated the application of iFRET and cell membrane microarrays for detecting membrane–membrane interactions, using cell membranes instead of living cells. This proof of concept was validated using the specific monoclonal antibody pembrolizumab, which induced the inhibition of PD-1/PD-L1 engagement between human PBMCs and melanoma membranes from the HT144 cell line or from a patient biopsy. These data show the potential of the developed assay to quantify other receptor–ligand interactions in the 1–10 nm range. The novelty and reproducibility of this approach, coupled with its lower time and labor requirements, will allow this assay to be applied to other fields, such as autoimmune disease, cancer, inflammation, and transplant rejection. This would consequently enable precise and periodic immune monitoring, thereby providing information to clinicians, which may result in personalized patient therapies.

Author Contributions: All authors had full access to all the data in the study and take responsibility for the integrity of the data and the accuracy of the data analysis. Study conceptualization and design, G.B.-G. and L.S.-M.; data acquisition, L.S.-M., M.d.l.F., C.E., J.M., A.E. and M.R.-A.; data analysis and interpretation, L.S.-M. and G.B.-G.; writing: original draft, all authors; critical revision of the manuscript for important intellectual content, all authors; funding acquisition, E.A. and G.B.-G.; study supervision, all authors. All authors have read and agreed to the published version of the manuscript.

Funding: This study was funded by the Spanish Ministry of Science and Innovation Center for Technological and Industrial Development (CDTI), CERVERA program, exp. 00119571, the Basque Government, BIKAINTEK program, exp. 201900007, and the Basque Government, HAZITEK program, exp. ZE201900012.

Institutional Review Board Statement: Not applicable.

Informed Consent Statement: Not applicable.

Data Availability Statement: Not applicable.

Acknowledgments: The authors thank Professor Larijani for her scientific discussions, conceptualization, and manuscript review, as well as Christopher Applebee for data acquisition and support with this project.

Conflicts of Interest: The authors declare no conflict of interest.

Appendix A

In order to assess the potential and robustness of using CMMAs, some examples of different assays developed are shown using consecutive CMMAs, as a comparison to those used for the PD-1/PD-L1 interaction studies. Bradford staining was used to confirm correct protein immobilization; additionally, mass spectrometric analysis of the lipid profile of each

sample was acquired to ensure that the lipid environment remained correct (Figure A1). MALDI-MS spectra of rat cortex (Cx) tissue had a similar peak profile to the 10 replicas of rat cortex tissue used as reference (Cx_Ref), confirming the integrity of the lipidic environment of the immobilized membrane. Furthermore, histamine receptor type 4 expression was determined in the samples included in the microarray using a specific anti-HR4 antibody with cross-reactivity between species, followed by an analysis of the functional coupling to G-proteins evoked by histamine receptors. Similar results were observed for the expression and functionality of the receptors (Figure A2). Moreover, the functional coupling triggered by histamine receptors was antagonized by haloperidol, confirming the specificity of the response, as well as the functionality of these membrane G-protein-coupled receptors. The HT144 sample featured a nonsignificant stimulation of the receptors when using histamine compared with basal levels, which was inhibited by haloperidol. The same was observed in rat cortex tissue and melanoma samples, with a significant stimulation in both cases when using histamine (p-value (***) < 0.001 for rat cortex tissue and p-value (*) < 0.05 for melanoma sample, using two-way ANOVA with Bonferroni correction). This stimulation was blocked in all samples when adding haloperidol as an antagonist (Figure A3). Lastly, the functional coupling triggered by WIN55212-2 and antagonized by AM251 was assayed using [^{35}S]GTPγS to confirm the functionality of CB1 cannabinoid receptors. In this assay, only rat cortex tissue showed a significant (p-value (*) < 0.05, using two-way ANOVA with Bonferroni correction) stimulation when using WIN55212-1 as a full agonist. This stimulation was antagonized by the specific CB1 receptor antagonist AM251 (Figure A4).

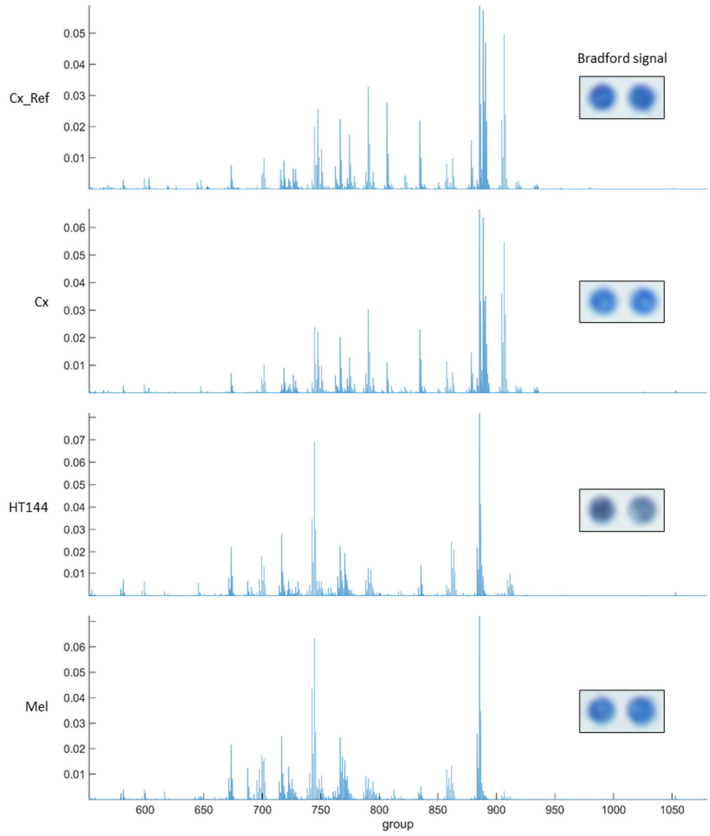

Figure A1. MALDI-MS average spectra of two replicas of rat cortex tissue (Cx), HT144 cells, and melanoma samples (Mel) fixated on a CMMA. The topmost image shows the average spectrum of 10 replicas of rat cortex tissue (Cx_Ref) measured using a different microarray. The Bradford signal of both replicas is included for each sample. The MALDI-MS imaging was carried out as described in [17,30], while the Bradford staining was carried out as described in [13,18].

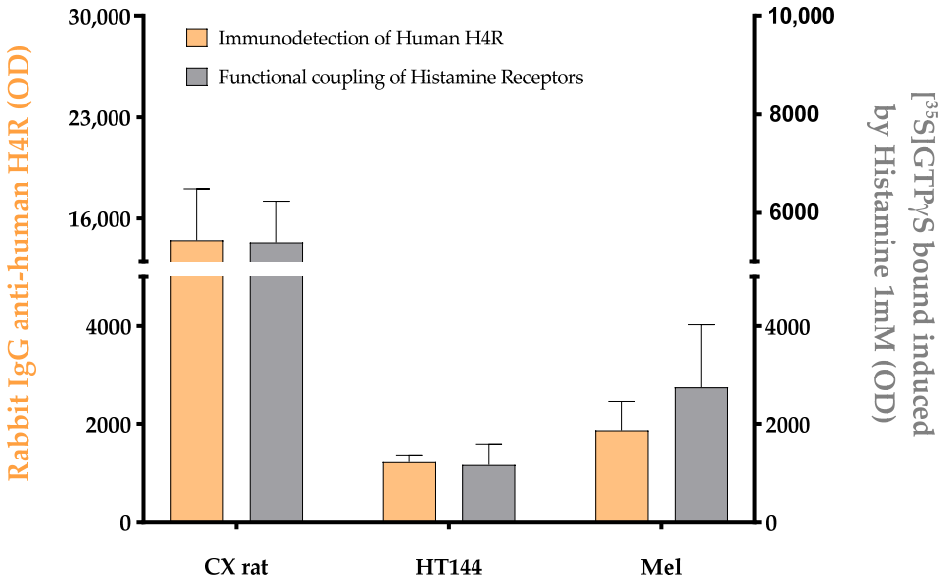

Figure A2. Human H4R receptor presence (orange) and functionality (gray) of two replicas of rat cortex tissue (Cx), HT144 cells, and melanoma samples (Mel) fixated on a CMMA. The presence of the receptor was determined using immunochemistry techniques, by incubating CMMA with rabbit IgG anti-human H4R 1:500 and labeling with a horseradish peroxidase-conjugated antibody against rabbit IgG. H4R functionality was assayed using [^{35}S]GTPγS binding protocols, as previously described in [13,31,32].

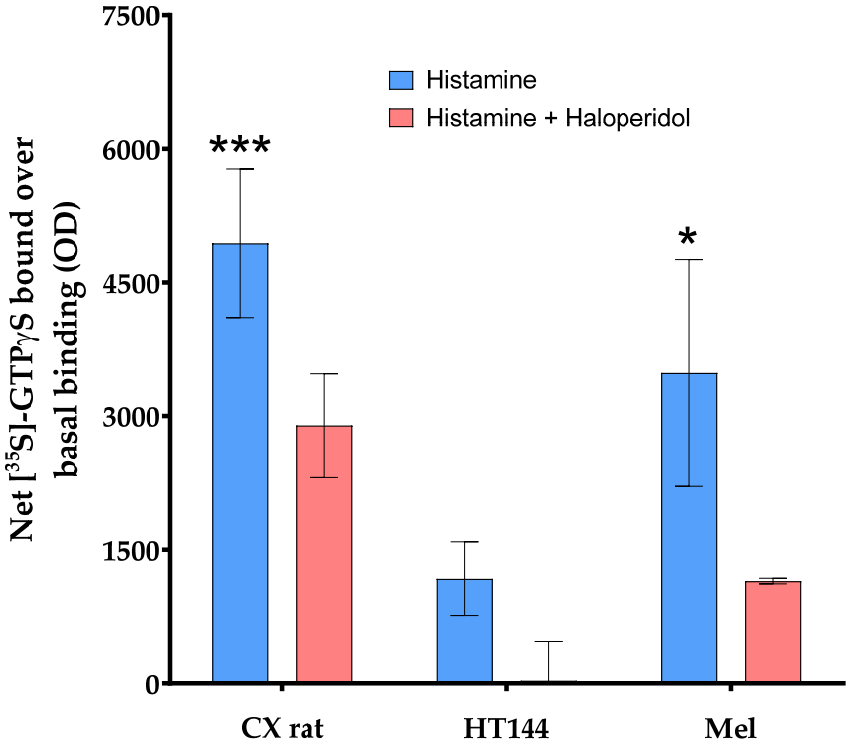

Figure A3. Effect of 1 mM histamine on the [^{35}S]GTPγS binding (blue) determined in membranes isolated from rat brain cortex tissue (CX rat), HT144 cells (HT144), and a melanoma biopsy (Mel) using CMMA. This effect was antagonized by 100 μM haloperidol (red). The assay was carried out as described in [32]. Two-way ANOVA with Bonferroni correction was applied as statistical test (p-value (***) < 0.001 and p-value (*) < 0.05).

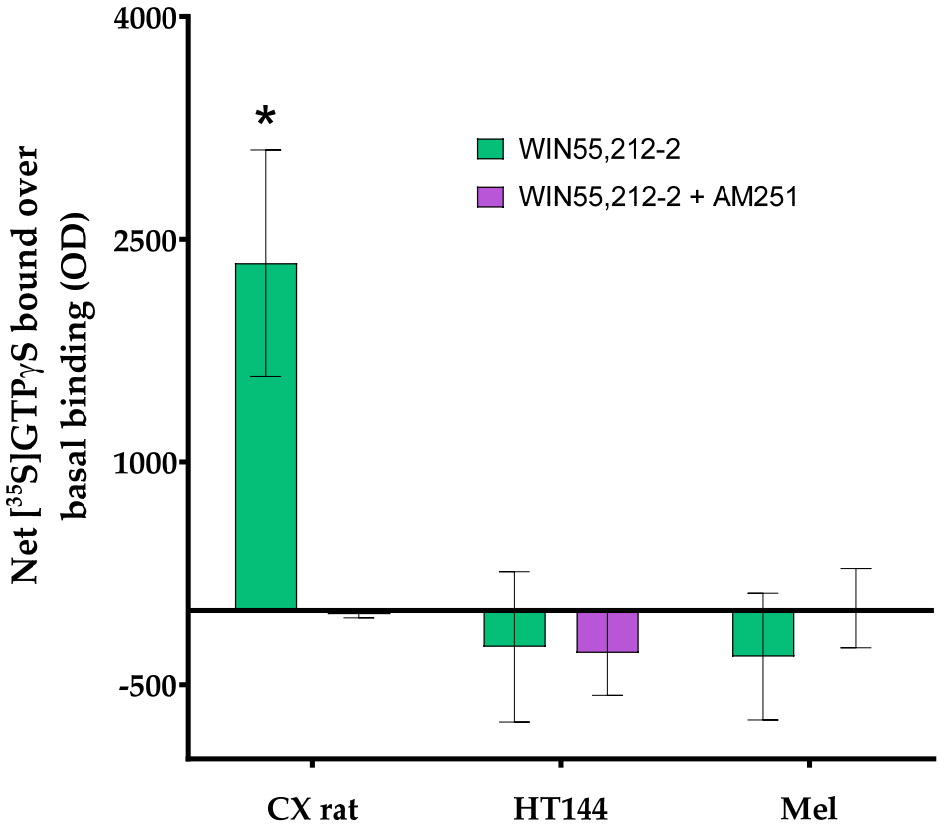

Figure A4. Effect of 10 μM WIN55212-2 (green) on the [^{35}S]GTPγS binding (blue) determined in membranes isolated from rat brain cortex tissue (CX rat), HT144 cells (HT144), and a melanoma biopsy (Mel) using CMMA. This effect was antagonized by 1 μM AM251 (purple). The assay was carried out as described in [12]. Two-way ANOVA with Bonferroni correction was applied as statistical test (p-value (*) < 0.05).

References

1. Okazaki, T.; Maeda, A.; Nishimura, H.; Kurosaki, T.; Honjo, T. PD-1 immunoreceptor inhibits B cell receptor-mediated signaling by recruiting src homology 2-domain-containing tyrosine phosphatase 2 to phosphotyrosine. *Proc. Natl. Acad. Sci. USA* **2001**, *98*, 13866–13871. [CrossRef]
2. Ding, H.; Wu, X.; Gao, W. PD-L1 is expressed by human renal tubular epithelial cells and suppresses T cell cytokine synthesis. *Clin. Immunol.* **2005**, *115*, 184–191. [CrossRef]
3. Carbone, D.P.; Gandara, D.R.; Antonia, S.J.; Zielinski, C.; Paz-Ares, L. Non-Small-Cell Lung Cancer:Role of the Immune System and Potential for Immunotherapy. *J. Thorac. Oncol.* **2015**, *10*, 974–984. [CrossRef]
4. Nunes-Xavier, C.E.; Angulo, J.C.; Pulido, R.; López, J.I. A Critical Insight into the Clinical Translation of PD-1/PD-L1 Blockade Therapy in Clear Cell Renal Cell Carcinoma. *Curr. Urol. Rep.* **2019**, *20*, 1. [CrossRef]
5. Bagchi, S.; Yuan, R.; Engleman, E.G. Immune Checkpoint Inhibitors for the Treatment of Cancer: Clinical Impact and Mechanisms of Response and Resistance. *Annu. Rev. Pathol.* **2021**, *16*, 223–249. [CrossRef]
6. Simeone, E.; Ascierto, P.A. Anti-PD-1 and PD-L1 antibodies in metastatic melanoma. *Melanoma Manag.* **2017**, *4*, 175–178. [CrossRef]
7. Angulo, J.C.; Shapiro, O. The Changing Therapeutic Landscape of Metastatic Renal Cancer. *Cancers* **2019**, *11*, 1227. [CrossRef]
8. Nunes-Xavier, C.E.; Zaldumbide, L.; Aurtenetxe, O.; López-Almaraz, R.; López, J.I.; Pulido, R. Dual-Specificity Phosphatases in Neuroblastoma Cell Growth and Differentiation. *Int. J. Mol. Sci.* **2019**, *20*, 1170. [CrossRef]
9. Stenzel, P.J.; Schindeldecker, M.; Tagscherer, K.E.; Foersch, S.; Herpel, E.; Hohenfellner, M.; Hatiboglu, G.; Alt, J.; Thomas, C.; Haferkamp, A.; et al. Prognostic and Predictive Value of Tumor-infiltrating Leukocytes and of Immune Checkpoint Molecules PD1 and PDL1 in Clear Cell Renal Cell Carcinoma. *Transl. Oncol.* **2020**, *13*, 336–345. [CrossRef]
10. Ribas, A.; Hamid, O.; Daud, A.; Hodi, F.S.; Wolchok, J.D.; Kefford, R.; Joshua, A.; Patnaik, A.; Hwu, W.-J.; Weber, J.; et al. Association of Pembrolizumab with Tumor Response and Survival Among Patients with Advanced Melanoma. *JAMA* **2016**, *315*, 1600–1609. [CrossRef]

11. Sánchez-Magraner, L.; Miles, J.; Baker, C.L.; Applebee, C.J.; Lee, D.-J.; Elsheikh, S.; Lashin, S.; Withers, K.; Watts, A.G.; Parry, R.; et al. High PD-1/PD-L1 Checkpoint Interaction Infers Tumor Selection and Therapeutic Sensitivity to Anti-PD-1/PD-L1 Treatment. *Cancer Res.* **2020**, *80*, 4244–4257. [CrossRef] [PubMed]
12. Hebert-Chatelain, E.; Desprez, T.; Serrat, R.; Bellocchio, L.; Soria-Gomez, E.; Busquets-Garcia, A.; Zottola, A.C.P.; Delamarre, A.; Cannich, A.; Vincent, P.; et al. A cannabinoid link between mitochondria and memory. *Nature* **2016**, *539*, 555–559. [CrossRef] [PubMed]
13. Fernández, R.A.; Garate, J.; Tolentino-Cortez, T.; Herraiz, A.; Lombardero, L.; Ducrocq, F.; Rodriguez-Puertas, R.; Trifilieff, P.; Astigarraga, E.; Barreda-Gómez, G.; et al. Microarray and Mass Spectrometry-Based Methodology for Lipid Profiling of Tissues and Cell Cultures. *Anal. Chem.* **2019**, *91*, 15967–15973. [CrossRef] [PubMed]
14. Rienda, B.; Elexpe, A.; Tolentino-Cortez, T.; Gulak, M.; Bruzos-Cidón, C.; Torrecilla, M.; Astigarraga, E.; Barreda-Gómez, G. Analysis of Acetylcholinesterase Activity in Cell Membrane Microarrays of Brain Areas as a Screening Tool to Identify Tissue Specific Inhibitors. *Analytica* **2021**, *2*, 25–36. [CrossRef]
15. Veeriah, S.; Leboucher, P.; De Naurois, J.; Jethwa, N.; Nye, E.; Bunting, T.; Stone, R.; Stamp, G.; Calleja, V.; Jeffrey, S.; et al. High-Throughput Time-Resolved FRET Reveals Akt/PKB Activation as a Poor Prognostic Marker in Breast Cancer. *Cancer Res.* **2014**, *74*, 4983–4995. [CrossRef]
16. Pereiro, X.; Fernández, R.; Barreda-Gómez, G.; Ruzafa, N.; Acera, A.; Araiz, J.; Astigarraga, E.; Vecino, E. Comparative lipidomic analysis of mammalian retinal ganglion cells and Müller glia in situ and in vitro using High-Resolution Imaging Mass Spectrometry. *Sci. Rep.* **2020**, *10*, 20053. [CrossRef]
17. Bradford, M.M. A rapid and sensitive method for the quantitation of microgram quantities of protein utilizing the principle of protein-dye binding. *Anal. Biochem.* **1976**, *72*, 248–254. [CrossRef]
18. Miles, J.; Applebee, C.J.; Leboucher, P.; Lopez-Fernandez, S.; Lee, D.-J.; Guarch, R.; Ward, S.; Parker, P.; López, J.I.; Larijani, B. Time resolved amplified FRET identifies protein kinase B activation state as a marker for poor prognosis in clear cell renal cell carcinoma. *BBA Clin.* **2017**, *8*, 97–102. [CrossRef]
19. Suárez, H.; Andreu, Z.; Mazzeo, C.; Toribio, V.; Pérez-Rivera, A.E.; López-Martín, S.; García-Silva, S.; Hurtado, B.; Morato, E.; Peláez, L.; et al. CD9 inhibition reveals a functional connection of extracellular vesicle secretion with mitophagy in melanoma cells. *J. Extracell. Vesicles* **2021**, *10*, e12082. [CrossRef]
20. Fogh, J.; Trempe, G. *New Human Tumor Cell Lines BT—Human Tumor Cells In Vitro*; Fogh, J., Ed.; Springer: Boston, MA, USA, 1975; pp. 115–159. [CrossRef]
21. Costantini, F.; Barbieri, G. The HLA-DR mediated signalling increases the migration and invasion of melanoma cells, the expression and lipid raft recruitment of adhesion receptors, PD-L1 and signal transduction proteins. *Cell. Signal.* **2017**, *36*, 189–203. [CrossRef]
22. Yi, M.; Niu, M.; Xu, L.; Luo, S.; Wu, K. Regulation of PD-L1 expression in the tumor microenvironment. *J. Hematol. Oncol.* **2021**, *14*, 10. [CrossRef]
23. Sunshine, J.C.; Nguyen, P.L.; Kaunitz, G.J.; Cottrell, T.R.; Berry, S.; Esandrio, J.; Xu, H.; Ogurtsova, A.; Bleich, K.B.; Cornish, T.C.; et al. PD-L1 Expression in Melanoma: A Quantitative Immunohistochemical Antibody Comparison. *Clin. Cancer Res.* **2017**, *23*, 4938–4944. [CrossRef]
24. Han, Y.; Liu, D.; Li, L. PD-1/PD-L1 pathway:current researches in cancer. *Am. J. Cancer Res.* **2020**, *10*, 727–742.
25. Söderberg, O.; Gullberg, M.; Jarvius, M.; Ridderstråle, K.; Leuchowius, K.-J.; Jarvius, J.; Wester, K.; Hydbring, P.; Bahram, F.; Larsson, L.-G.; et al. Direct observation of individual endogenous protein complexes in situ by proximity ligation. *Nat. Methods* **2006**, *3*, 995–1000. [CrossRef] [PubMed]
26. Söderberg, O.; Leuchowius, K.-J.; Gullberg, M.; Jarvius, M.; Weibrecht, I.; Larsson, L.-G.; Landegren, U. Characterizing proteins and their interactions in cells and tissues using the in situ proximity ligation assay. *Methods* **2008**, *45*, 227–232. [CrossRef] [PubMed]
27. Tu, S.; Jiang, H.-W.; Liu, C.-X.; Zhou, S.-M.; Tao, S.-C. Protein Microarrays for Studies of Drug Mechanisms and Biomarker Discovery in the Era of Systems Biology. *Curr. Pharm. Des.* **2014**, *20*, 49–55. [CrossRef]
28. Wegener, J. Cell-Based Microarrays for In Vitro Toxicology. *Annu. Rev. Anal. Chem.* **2015**, *8*, 335–358. [CrossRef] [PubMed]
29. Yang, L.; Guo, S.; Li, Y.; Zhou, S.; Tao, S. Protein microarrays for systems biology. *Acta Biochim. Biophys. Sin.* **2011**, *43*, 161–171. [CrossRef] [PubMed]
30. Manuel, I.; Barreda-Gómez, G.; Román, E.G.D.S.; Veloso, A.; Fernandez, J.; Giralt, M.T.; Rodríguez-Puertas, R. Neurotransmitter Receptor Localization: From Autoradiography to Imaging Mass Spectrometry. *ACS Chem. Neurosci.* **2015**, *6*, 362–373. [CrossRef] [PubMed]
31. Barreda-Gómez, G.; Giralt, M.; Rodriguez-Puertas, R. Effects of central galanin administration on muscarinic cholinergic and galanin receptor G protein coupling. *Neuropeptides* **2005**, *39*, 157–160. [CrossRef]
32. Papon, M.-A.; Le Feuvre, Y.; Barreda-Gómez, G.; Favereaux, A.; Farrugia, F.; Bouali-Benazzouz, R.; Nagy, F.; Rodríguez-Puertas, R.; Landry, M. Spinal Inhibition of GABAB Receptors by the Extracellular Matrix Protein Fibulin-2 in Neuropathic Rats. *Front. Cell. Neurosci.* **2020**, *14*, 214. [CrossRef] [PubMed]